ACS APPLIED NANO MATERIALS
Cite This: ACS Appl. Nano Mater. 2019, 2, 566−576
Article
www.acsanm.org

# In Situ Functionalized Fluorescent $WS_2$-QDs as Sensitive and Selective Probe for $Fe^{3+}$ and a Detailed Study of Its Fluorescence Quenching

Vijay K. Singh,[†] Himanshu Mishra,[†] Rashid Ali,[‡] Sima Umrao,[§] Rajesh Srivastava,[†] Shiju Abraham,[#] Arvind Misra,[‡] Vidya Nand Singh,[⊥] Hirdyesh Mishra,[∥] R. S. Tiwari,*[,†] and Anchal Srivastava*[,†]

[†]Department of Physics, Institute of Science, Banaras Hindu University, Varanasi 221005, India
[‡]Department of Chemistry, Institute of Science, Banaras Hindu University, Varanasi 221005, India
[§]Department of Mechanical Engineering, School of Mechanical and Aerospace Engineering, Korea Advanced Institute of Technology (KAIST), Dajeon 34141, South Korea
[∥]Department of Physics (MMV), Banaras Hindu University, Varanasi 221005, India
[⊥]CSIR-National Physical Laboratory, Dr. K. S. Krishnan Marg, New Delhi 110012, India
[#]The Zuckerberg Institute for Water Research, The Jacob Blaustein Institutes for Desert Research, Ben-Gurion University of the Negev, Sede Boqer 8499000, Israel

Supporting Information

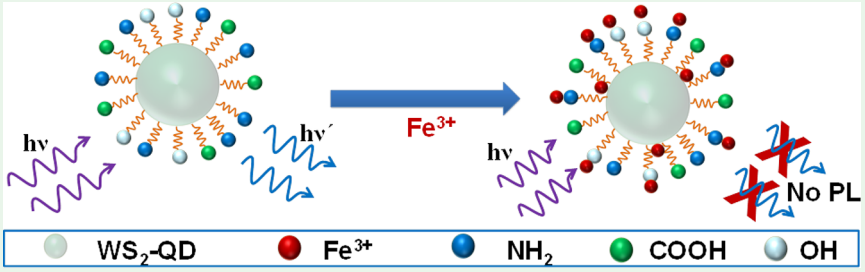


**ABSTRACT:** Most of the reports suggest that liquid exfoliated $WS_2$-QDs are unstable; therefore the need of present day is to develop a novel synthesis route for producing long-term stable $WS_2$-QDs. Herein, we report a bottom-up single-step hydrothermal growth of in situ functionalized blue fluorescent $WS_2$-QDs with stable fluorescence in aqueous media without subsequent treatments. Presence of various functional groups over the surface of f-$WS_2$-QDs provides high solubility and stability to f-$WS_2$-QDs in aqueous media preserving its fluorescence. Further, photoluminescence property of f-$WS_2$-QDs has been employed to devise an optical sensor with a high sensitivity ($K_D \sim 10^4\ M^{-1}$) and selectivity for ferric ($Fe^{3+}$) ions. Under the optimal condition, response of the sensor is found to be linear in the range of 0−55 $\mu$M with a limit of detection (LOD) of 1.32 $\mu$M, which is within the maximum permissible level of $Fe^{3+}$ (~5.4 $\mu$M) in human drinking water by the USEPA. Further, we have also carried out a detailed evaluation on fluorescence quenching kinetics of f-$WS_2$-QDs. Nonlinear behavior of S−V plot and TRPL measurements suggest that quenching is a mixed phenomenon of dynamic as well as static processes. Finally we have proposed a mechanism for fluorescence quenching of f-$WS_2$-QDs in the presence of $Fe^{3+}$.

**KEYWORDS:** *$WS_2$, quantum dots, hydrothermal synthesis, quantum yield, TRPL, fluorescence quenching*

## INTRODUCTION

In the post-graphene era, a great sensation has been observed in the current research on layered transition metal dichalcogenides (LTMDs) of few-to-monolayer nanocrystals (NCs) or quantum dots (QDs) of $MoS_2$, $WS_2$, $MoSe_2$, etc., which have been conceived as best substitutes of graphene and carbon QDs.[1−4] In this LTMDs series, 2D $WS_2$ has aroused even greater attention owing to its controllable band gaps as a function of layer numbers with remarkable optical and electronic properties.[5−7] $WS_2$ is a van der Waals layered material with hexagonal lattice structure arranged in triple layers (S−W−S); each layer has a thickness of 6 Å with strong in-plane covalent bonding and weak out-of-plane van der Waals interactions.[8] Further, by reducing the lateral size of 2D $WS_2$ sheet in 0D $WS_2$-QDs, one can acquire excellent electrical/optical behaviors from these NCs due to their strong quantum confinement and edge effects.[9] In addition to this, $WS_2$-QDs possess larger surface to volume ratio and much more active sites beyond monolayer 2D $WS_2$, which may be beneficial for sensing, catalysis, bioimaging, etc. To date,

Received: November 28, 2018
Accepted: December 14, 2018
Published: December 14, 2018






DOI: 10.1021/acsanm.8b02162
ACS Appl. Nano Mater. 2019, 2, 566−576

several "top-down" routes have been reported for producing $WS_2$-QDs, which include liquid phase exfoliation, intercalated exfoliation of bulk $WS_2$ followed by hydrothermal scissoring, ultrasonication, etc.[4,10−13] For instance, Lin et al. synthesized $WS_2$-QDs using potassium ions ($K^+$) intercalation of bulk $WS_2$ flakes followed by ultrasonication.[9] However, removal of the $K^+$ ions led to the instability to $WS_2$-QDs.[2,9,13] Zhao et al. reported synthesis of $WS_2$-QDs by exfoliating bulk $WS_2$ through $H_2SO_4$ intercalation.[14] This method requires a tedious and time-consuming post-treatment of lipoic acid conjugated poly(ethylene glycol) on the surface of $WS_2$-QDs. Zhang et al. synthesized $WS_2$-QDs through ultrasonic crushing of $WS_2$ powder for 12 h. But this synthesis approach also requires a second step of L-cysteine coating over $WS_2$-QDs surface for their protection.[15] In another report Xian et al. described the synthesis of water-soluble $WS_2$-QDs through ultrasonication of $WS_2$ powder in the presence of CTAB followed by hydrothermal scissoring.[10] CTAB (ionic surfactant) stabilizes $WS_2$-QDs in water and prevents its agglomeration; however, it is known to possess cytotoxicity which is not suitable for biological applications. Besides these, several other reports are available showing the importance of surface passivation/functionalization of QDs to make them stable and biocompatible. However, all these reported methods followed tedious and time-consuming post-processing of the sample to achieve the same. Moreover, earlier reports also suggest that QDs without passivation or surface functionalization lead to weak fluorescence due to agglomeration.[16,17] Therefore, for the best exploitation of $WS_2$-QDs potential, it must remain fluorescent and stably dispersed in water and biological fluids, which can be achieved through surface passivation/functionalization of it. Thus, there is a great challenge to develop a cost-effective, environment friendly, facile, and high yield strategy to produce water-soluble in situ functionalized $WS_2$-QDs with stable fluorescence.

$Fe^{3+}$ is the most important and essential ion for the metabolic process of all the living systems. It is involved in oxygen metabolism, and by virtue of its redox chemistry as well as high affinity for oxygen, it facilitates electron transfer in DNA and RNA synthesis.[18] Its deficiency and excess both from normal permissible level can induce a variety of diseases. For example, iron deficiency (hypoferremia) causes anemia, liver damage, diabetes, cancer, and Parkinson's diseases and accumulation of iron (hyperferremia) causes oxidative stress, hemochromatosis, and Alzheimer's and neurodegenerative diseases due to over production of $H_2O_2$, etc.[19,20] Inappropriate treatment of metal ions can also lead to metal ion contamination, which has become a critical environmental issue in developing countries. Hence, the determination of $Fe^{3+}$ in the biological systems and aquatic environment is of burgeoning interest for effectively monitoring and controlling the metal ion concentration. In this aspect, the development of metal ion sensors is a hot, yet challenging topic. In this context, many efforts have been devoted for developing accurate, sensitive, and selective approaches for metal ion detection, such as inductively coupled plasma mass spectrometry, voltammetry, fluorescent sensor, etc.[21−23] Among these, fluorescence based sensor is most appealing due to its inherent simplicity, high sensitivity, and freedom from sophisticated instrumentations.[18,24]

Although $MoS_2$-QDs has been synthesized using hydrothermal method,[25−27] however to the best of our knowledge, for the first time, we demonstrate a novel, scalable single-step "bottom-up" hydrothermal approach for producing nanometer sized, good quality, monodispersed in situ functionalized fluorescent $WS_2$-QDs. Owing to its nanometer size, the as-synthesized f-$WS_2$-QDs give highly intense blue fluorescence ($\lambda \sim 410$ nm) in UV-light which can be easily visualized by naked eye under UV lamp (~365 nm). The reagents used in present synthesis approach are $Na_2WO_4{\cdot}2H_2O$ and L-cysteine. Also the present method does not require any additional surface passivation agents and post-synthesis processing, which makes it more attractive as compared to the other reports on the synthesis of $WS_2$-QDs.[9,10] L-Cysteine causes the self-passivation of QDs and hence provides stability to the QDs in aqueous media. Further, for the proof of concept we have also demonstrated that our as-produced f-$WS_2$-QDs have potential to be applied as fluorescent probe for highly sensitive ($K_D \sim 10^4$ $M^{-1}$) and selective detection of $Fe^{3+}$ ions. Under the optimal condition response of the sensor is found to be linear in the range of 0−55 $\mu$M with a LOD of 1.32 $\mu$M. Apart from this, we have also carried out a detailed kinetic study to unveil the interaction between f-$WS_2$-QDs and $Fe^{3+}$ ions. S−V plot and time-resolved photoluminescence (TRPL) study reveal that fluorescence quenching is a mixed phenomenon of both static and dynamic processes. We have also proposed a mechanism for fluorescence quenching of f-$WS_2$-QDs in the presence of $Fe^{3+}$.

## EXPERIMENTAL SECTION

**Reagents and Chemicals.** All the reagents used in the present work were of analytical grade and used without any further purification. Sodium tungstate dihydrate ($Na_2WO_4.2H_2O$) was obtained from Hi-media Chemicals, India. It was used as starting material for the synthesis of f-$WS_2$-QDs. L-Cysteine and hydrochloric acid (HCl) were procured from Merck, India, and Molychem Chemicals India, respectively. Deionized (DI) water was used as solvent material in hydrothermal synthesis as well as for all the optical and sensing measurements of f-$WS_2$-QDs. The stock solutions of different metal ions (0.1 M) such as $Na^+$, $K^+$, $Ca^{2+}$, $Al^{3+}$, $Cd^{2+}$, $Zn^{2+}$, $Ni^{2+}$, $Hg^{2+}$, $Fe^{2+}$, $Pb^{2+}$, $Cu^{2+}$, and $Fe^{3+}$ were freshly prepared by dissolving their nitrate salts in water.

**Techniques Used for Material Characterizations.** Transmission electron microscopic (TEM) and high-resolution transmission electron microscopic (HR-TEM) images of f-$WS_2$-QDs were obtained through Tecnai G2 TEM (FEI, USA) operated at 200 kV. The atomic force microscopic (AFM) image of f-$WS_2$-QDs was acquired using JPK NanoWizard 4 (JPK Instruments AG, Germany) using gold-coated silicon tips (tip radius, 2−12 nm) (SNL-10 probe; Camarillo, CA) with a spring constant of 0.35 N/m in quantitative imaging (QI) mode. For AFM imaging, the sample was drop-cast on a freshly cleaved mica surface. For the evidence of the chemical composition of the f-$WS_2$-QDs, X-ray photoelectron spectra (XPS) were recorded in multiprobe surface analysis system (ESCA2000 VG Microtech Inc.) using monochromatic Mg K$\alpha$ (1253.6 eV) radiation source. The base pressure of the instrument was maintained in the range of $10^{-10}$−$10^{-11}$ Torr during the sample analysis. The pass energy of the scans was fixed at 10 eV with a spectral resolution of ~0.1 eV. All the reported binding energies in the present work are calibrated to the C 1s peak at 284.6 eV. Raman spectra of the as-synthesized f-$WS_2$-QDs were recorded at room temperature with a Renishaw inVia Raman spectrophotometer (Germany), equipped with a diode pump solid-state laser of wavelength 532 nm. Laser beam was incident on the sample with a 50× objective at a constant laser power of 5 mW $mm^{-2}$. Absorption spectra of as-synthesized material were recorded using UV−vis spectrophotometer (PerkinElmer, USA) having a quartz cuvette of standard 10 mm path length. Static photoluminescence (PL) and lifetime spectra of f-$WS_2$-QDs were recorded using fluorescence spectrophotometer (PerkinElmer, USA)


DOI: 10.1021/acsanm.8b02162
ACS Appl. Nano Mater. 2019, 2, 566−576

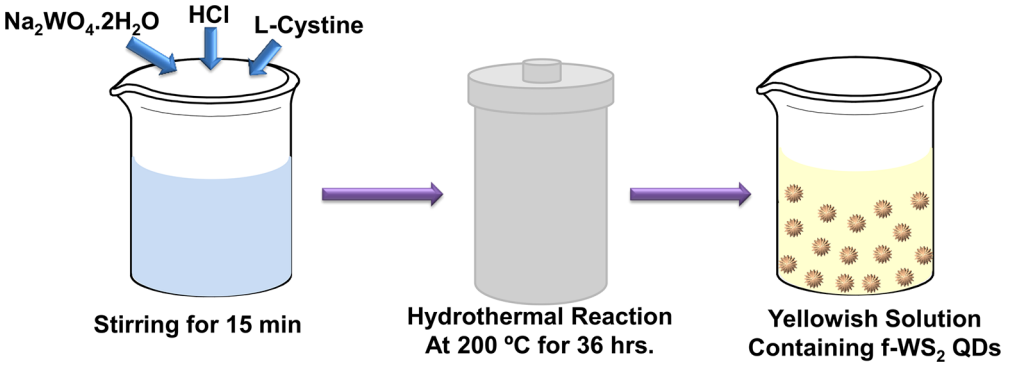


**Figure 1.** Schematic illustration showing the hydrothermal synthesis of f-$WS_2$-QDs.

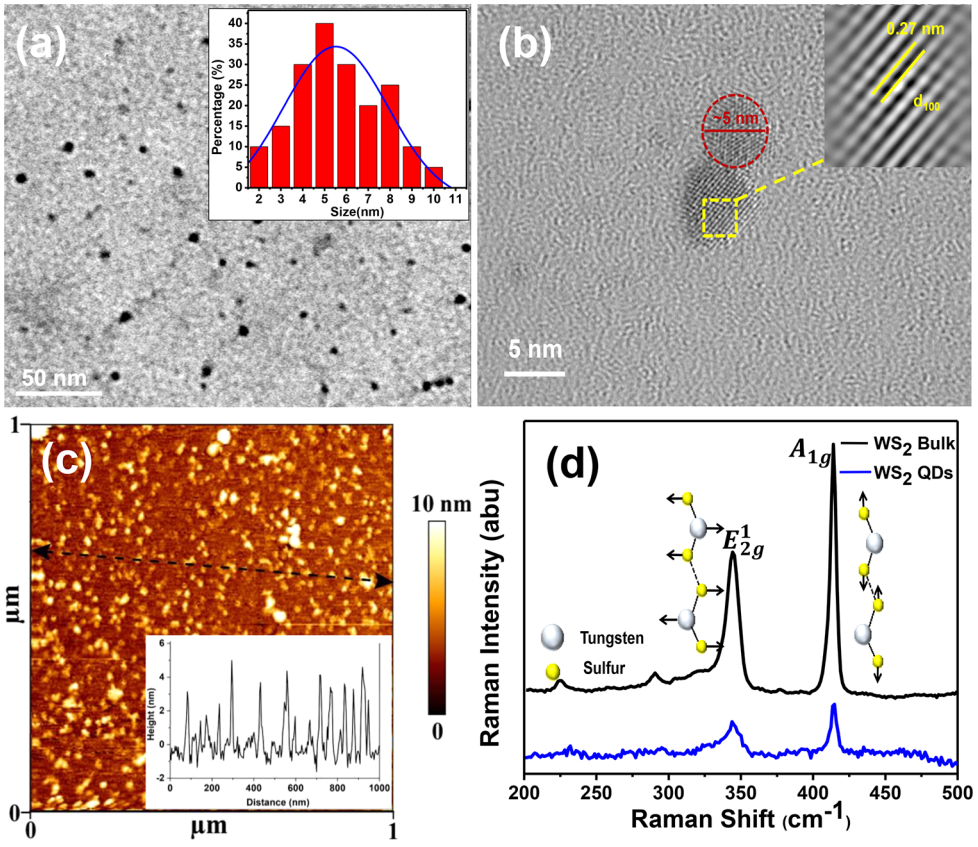


**Figure 2.** (a, b) TEM and HR-TEM images showing highly dispersed and crystalline f-$WS_2$-QDs. (c) AFM image and height profile (along the black line) of f-$WS_2$-QDs dispersed on mica sheet showing the monodispersed QDs with average height of ~4 nm. (d) Raman spectra of bulk as well as QDs of $WS_2$ showing characteristic peaks $E^1_{2g}$ and $A_{1g}$ phonon modes corresponding to the in-plane and out-of-plane vibrations of S−W−S atoms.

and time-resolved photoluminescence (TRPL) spectrophotometer (FLS920, Edinburgh, UK), respectively.

**Synthesis of f-$WS_2$-QDs.** As shown in Figure 1, f-$WS_2$-QDs were synthesized using a single step, facile, and scalable hydrothermal synthesis approach. Typically, 0.25 g of $Na_2WO_4{\cdot}2H_2O$ was dissolved in 25 mL of DI water. After the mixture was stirred for 15 min, the pH value of the solution was adjusted to ~4.0 using 0.1 M HCl solution. Further, 0.5 g of L-cysteine dissolved in 50 mL of distilled water separately was poured in the solution and sonicated for 10 min. Finally, the as-prepared solution was transferred into 100 mL Teflon-lined stainless steel hydrothermal vessel. After heating at 200 °C for 36 h followed by cooling down to room temperature, yellowish color solution containing f-$WS_2$-QDs was obtained. The proposed reaction during the hydrothermal synthesis is as follows:

$$HSCH_2CHNH_2COOH + H_2O \rightarrow CH_3COCOOH + NH_3 + H_2S \quad (R1)$$

$$4WO_4^{2-} + 9H_2S + 6CH_3COCOOH \rightarrow 4WS_2 + SO_4^{2-} + 6CH_3COCOO^- + 12H_2O \quad (R2)$$

**Sensing Procedure of Metal Ions ($Fe^{3+}$) Using f-$WS_2$-QDs.** Fluorescence quenching based sensitive and selective detection of $Fe^{3+}$ using f-$WS_2$-QDs as fluorescent probe has been investigated. The metal ions interaction study was performed by the addition of freshly prepared solution of metal ions (0.1 M) into the quartz cuvette containing 3.0 mL solution of f-$WS_2$-QDs. After homogenization, the change in fluorescence intensity was recorded for the wavelength of ~410 nm under the excitation wavelength of ~310 nm. In addition to


DOI: 10.1021/acsanm.8b02162
ACS Appl. Nano Mater. 2019, 2, 566−576

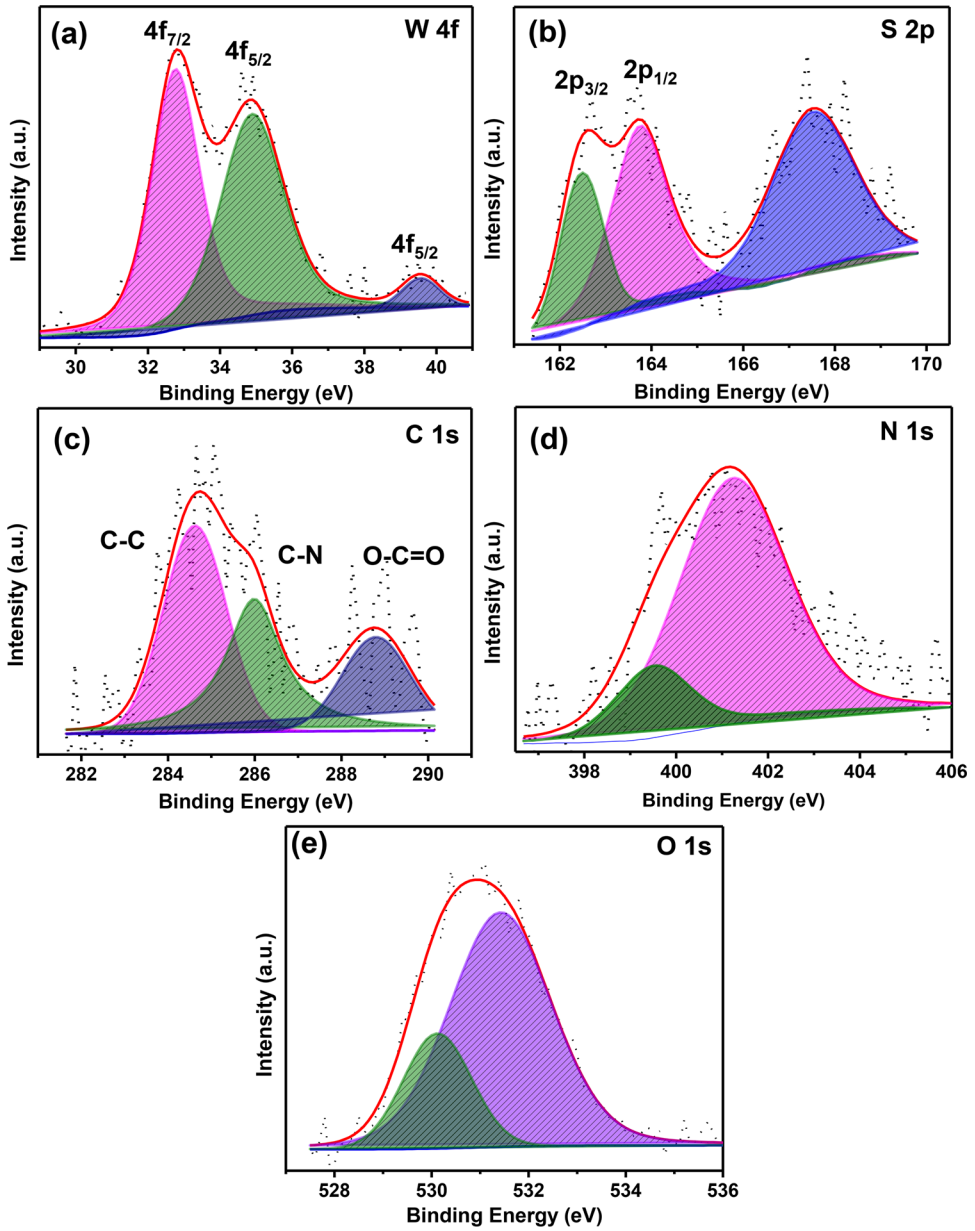


**Figure 3.** (a) W 4f, (b) S 2p, (c) C 1s, (d) N 1s, and (e) O 1s high resolution XPS spectra of f-$WS_2$-QDs.

this, the selectivity of sensing probe (f-$WS_2$-QDs) for $Fe^{3+}$ was analyzed by addition of different metal ions to the solution of f-$WS_2$-QDs containing $Fe^{3+}$ ions.

## RESULTS AND DISCUSSION

As-prepared f-$WS_2$-QDs were characterized using various techniques such as TEM, HRTEM, AFM, and Raman spectroscopy to confirm and highlight their structural properties. Figure 2a shows TEM image of f-$WS_2$-QDs, revealing that as-prepared f-$WS_2$-QDs are uniform and monodispersed in nature. Variations in particle size have been plotted and presented in the inset of Figure 2a, which is well fitted with the Gaussian distribution function giving an average particle size of ~5.0 nm ($n$ = 75). From here we can anticipate that such narrow distribution in particle size with superior homogeneous dispersion can significantly enhance the sensing performance of f-$WS_2$-QDs. High-resolution TEM (HR-TEM) image of typical f-$WS_2$-QDs (Figure 2b) confirms the growth of highly crystalline f-$WS_2$-QDs with a particle diameter of ~5 nm. A crystal lattice $d$-spacing (inset of Figure 2b) is identified to be 0.27 nm, which corresponds to the (100) lattice plane of f-$WS_2$ crystal.[28,29]

Furthermore, AFM analysis was performed to see the morphology and thickness of the as-synthesized f-$WS_2$-QDs. The topographic image and height profile obtained through AFM have been shown in Figure 2c. Similar to the TEM result, AFM analysis also reveals that QDs are monodispersed in nature. The height profile in Figure 2c shows the height of f-$WS_2$-QDs is ~4 nm, which confirms that QDs are few layered (~4−5 layers). Raman spectroscopic technique has been widely adopted for the characterization of the vibrational properties of TMDs and other layered materials because of its proven sensitivity and nondestructive nature. So we have also employed this technique to study the thickness and the vibrational modes present in the f-$WS_2$-QDs. Raman spectra of f-$WS_2$-QDs as well as its bulk counterpart have been shown in Figure 2d. In bulk $WS_2$ as well as in f-$WS_2$-QDs two prominent


DOI: 10.1021/acsanm.8b02162
ACS Appl. Nano Mater. 2019, 2, 566−576

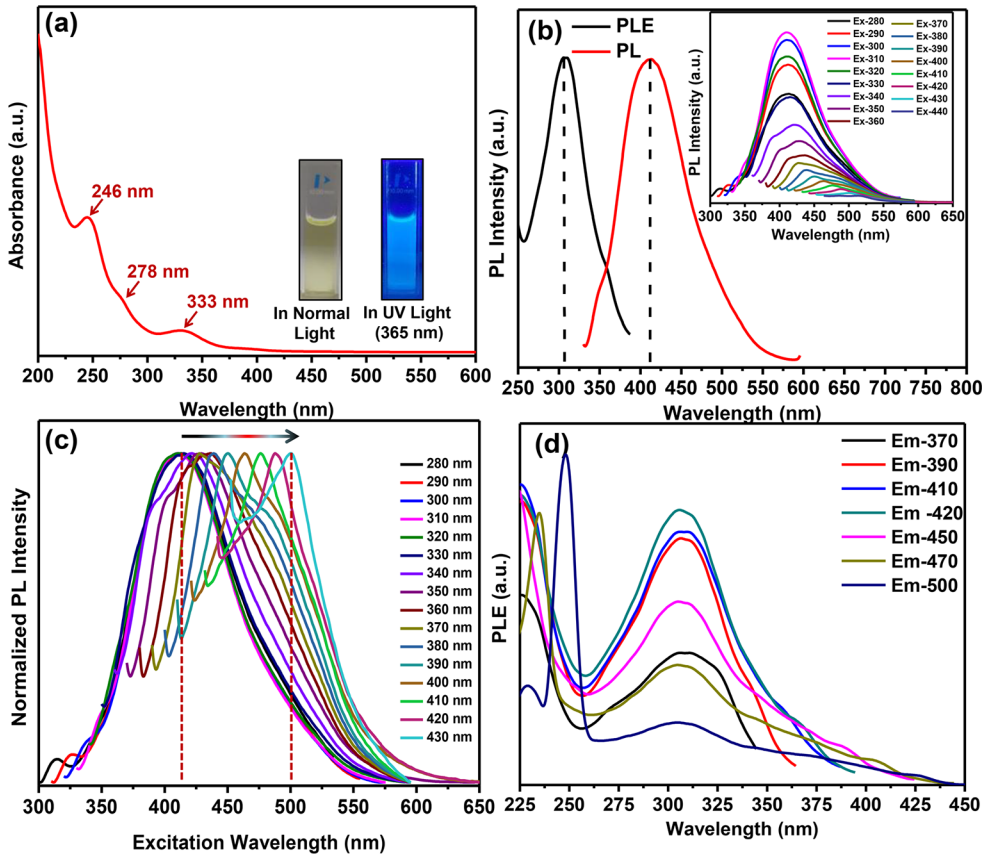


**Figure 4.** Photophysical properties of f-$WS_2$-QDs: (a) UV−vis absorption spectra and inset showing the f-$WS_2$-QDs liquid under normal and UV (~365 nm) light; (b) spectroscopic overlap between PL excitation spectra (PLE, black line, for an emission wavelength $\lambda_{em}$ = 410 nm) and PL emission spectra (red line, for an excitation wavelength $\lambda_{ex}$ = 310 nm) and inset showing PL spectra of f-$WS_2$-QDs at various excitation wavelengths; (c) normalized PL plot of excitation dependent PL spectra and (d) PL excitation (PLE) spectra for various emission wavelengths ranging from 370 to 500 nm.

peaks around ~348 $cm^{-1}$ and ~418 $cm^{-1}$ are observed, which correspond to the $E^1_{2g}$ and $A_{1g}$ phonon modes of 2H-$WS_2$, respectively, where $E^1_{2g}$ and $A_{1g}$ correspond to the in-plane and out-of-plane vibrations of S−W−S atoms, respectively.[30] It is evident from Figure 2d that the intensities of these peaks are much weaker in case of f-$WS_2$-QDs. The decrement in absolute intensity is due to the weaker interlayer attraction (water molecule interaction), which causes very narrow contribution toward the phonon restoring forces.[10] In addition to these, Fourier transform infrared (FTIR) spectroscopy was also performed to investigate the bonding composition of f-$WS_2$-QDs and presence of functional groups over the surface of these QDs (Figure S1). FTIR spectra confirmed the presence of various functional groups −COOH, $-NH_2$, −OH, $-SO_4^{2-}$, etc. over the surface of f-$WS_2$-QDs.

**XPS Characterization.** An XPS characterization was carried out to analyze the surface compositions and bonding characteristics of the as-synthesized f-$WS_2$-QDs. The high resolution core level spectra of W 4f, S 2p, C 1s, and O 1s have been shown in Figure 3. The region with binding energy (BE) from 30 to 38 eV can be fitted into doublet peaks located at 32.8 and 34.9 eV (Figure 3a), which can be attributed to the W $4f_{7/2}$ and W $4f_{5/2}$, respectively. These peaks are consistent with $W^{4+}$ oxidation state of W in f-$WS_2$-QDs.[31] An additional peak at 39.3 eV is attributed to the $W^{6+}$ oxidation state of W in tungsten hydroxide, which might be formed due to the surface oxidation of QDs during the hydrothermal synthesis process.[9,10] The BE of 2p core level of S in the range of 161 to 166 eV can be fitted into doublet peaks at 162.5 and 163.7 eV, which can be attributed to the S $2p_{3/2}$ and S $2p_{1/2}$ of $S^{2-}$, respectively (Figure 3b), suggesting the formation of $WS_2$. The peak at 167.9 eV signifies the presence of sodium sulfate, which is supposed to be present as residue after reaction in the colloidal suspension of f-$WS_2$-QDs.[32,33] The BE of C 1s spectra in range of 280−290 eV can be deconvoluted into three peaks at 284.6, 285.9, and 288.9 eV (shown in Figure 3c), which can be attributed to the C−C, C−N, and O−C═O, respectively. The BE of N 1s spectra in the range of 397−406 eV is deconvoluted into two peaks at 399.5 and 401.3 eV (shown in Figure 3d), which might be attributed to the C−N and O═C−N, respectively. These peaks confirm the presence of various functional groups such as carbonyl, carboxylic, etc. over the surface of as-synthesized $WS_2$-QDs,[34] which is also in good agreement with the FTIR analysis. Further, the BE of O 1s core level peak in the region 528−535 eV can be fitted into doublet peaks at 530.1 and 531.4 eV (shown in Figure 3d). The peak with BE = 530.1 eV can be assigned to the oxygen atoms ($O^{2-}$) of W═O bonds, and the peak with BE = 531.4 eV corresponds to the O−H group.[35] The presence of W═O and O−H group also confirms that edge of QDs is oxidized, which provides stability to it in water solution. From the XPS analysis we found that atom % values of $W_{4f}$ and $S_{2p}$ are 7.53 and 13.1, respectively. It shows that W and S atoms are in the ratio of approximately 1:2, which should be exactly 1:2 for pure


DOI: 10.1021/acsanm.8b02162
ACS Appl. Nano Mater. 2019, 2, 566−576

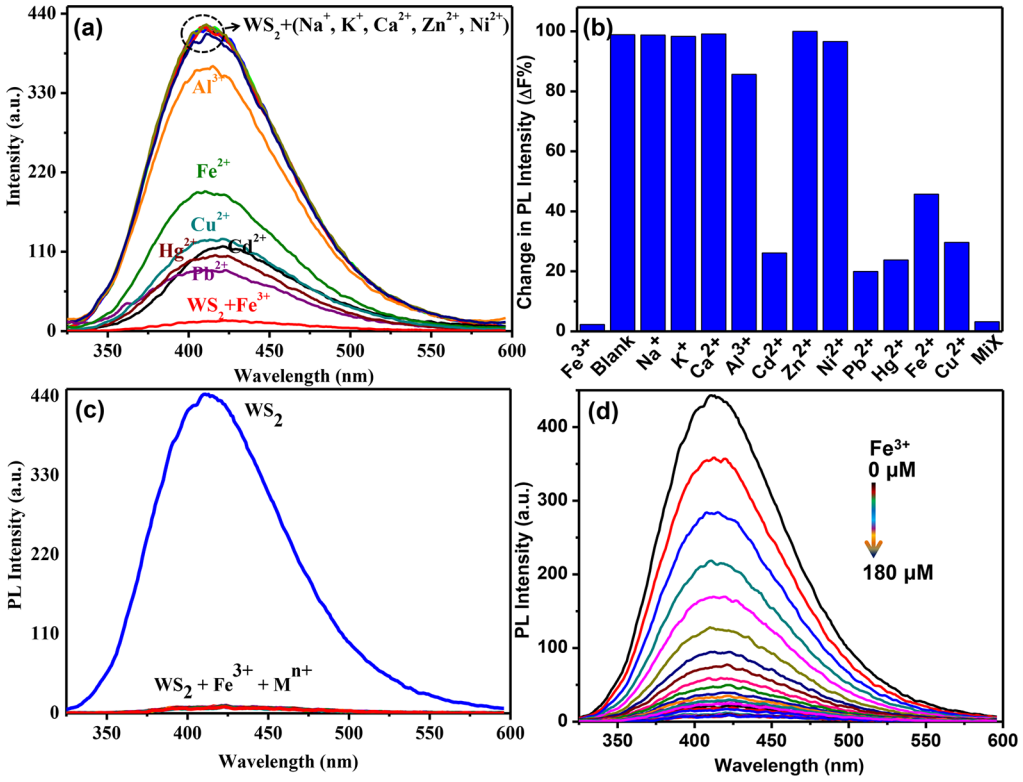


**Figure 5.** PL spectra of f-$WS_2$-QDs (a) upon interaction with various metal ions (180.0 $\mu$M), (b) percentage change in fluorescence intensity of f-$WS_2$-QDs in the presence of various metal ions, (c) interference of different metal ions to a solution of f-$WS_2$-QDs + $Fe^{3+}$, and (d) PL titration spectra of f-$WS_2$-QDs upon a gradual addition of $Fe^{3+}$ (0−180.0 $\mu$M).

$WS_2$ crystal. This sulfur deficiency may be attributed to the surface oxidation of $WS_2$-QDs.

**Photophysical Properties of f-$WS_2$-QDs.** In order to unveil the photophysical properties of the as-synthesized f-$WS_2$-QDs, UV−vis absorption and photoluminescence (PL) characterizations were carried out, which have been shown in Figure 4. The absorption spectra of as-prepared f-$WS_2$-QDs is represented in Figure 4a, in which two intense absorption bands at 333 nm (3.72 eV) and 246 nm (5.04 eV), a hump at 278 nm (4.46 eV) along with a weak absorption at the red edge of the absorption spectra are observed. The band at 333 nm is attributed to the excitonic absorption band of f-$WS_2$-QDs arising from direct gap transitions at the K point. The absorption band at 278 nm (4.46 eV) is attributed to the optical transitions from the valence band to the conduction band.[9] The band at 246 nm (5.04 eV) might be attributed to the surface defects as well as surface adsorbed functional groups ($-NH_2$, $-SO_4^{2-}$, $-OH^-$, etc.) of f-$WS_2$-QDs.[26] A visual inspection shows that in normal light f-$WS_2$-QDs solution appears as light yellow in color, while it gives highly intense blue fluorescence under UV-lamp ($\lambda$ = 365 nm) (inset of Figure 4a). To confirm this, the room temperature PL spectra of f-$WS_2$-QDs were recorded with PL spectrophotometer. Figure 4b shows the PL emission spectra recorded at various excitation wavelengths ($\lambda_{ex}$) ranging from 280 to 430 nm. It is observed that initially PL intensity increases when $\lambda_{ex}$ varied from 280 to 310 nm and after that it starts decreasing (inset of Figure 4b); maximum PL intensity was observed at emission wavelength $\lambda_{em}$ ∼ 410 nm with $\lambda_{ex}$ ∼ 310 nm. It is also observed that at higher excitation wavelengths PL peak shifted toward the red edge of emission spectra. To verify this nature, the normalized PL intensities for different excitation wavelengths have been plotted and shown in Figure 4c. It clearly indicates the edge excitation red shifting of 90 nm starting from 410 to 500 nm. This edge excitation red shifting property indicate the polydispersity nature of f-$WS_2$-QDs. Further, photoluminescence excitation (PLE) spectra of f-$WS_2$-QDs for different $\lambda_{em}$ ranging from 370 to 500 nm were also recorded and shown in Figure 4d. Weak excitation peaks at the red edge of the PLE spectra also support the edge excitation red shifting observed in PL spectra.

**Detection of Ferric Ions ($Fe^{3+}$) by Using f-$WS_2$-QDs.** The sensing behavior of f-$WS_2$-QDs in the presence of different metal ions such as $Na^+$, $K^+$, $Al^{3+}$, $Ca^{2+}$, $Fe^{2+}$, $Fe^{3+}$, $Ni^{2+}$, $Cu^{2+}$, $Zn^{2+}$, $Cd^{2+}$, $Hg^{2+}$, and $Pb^{2+}$ (as their nitrate salts) has been examined through the PL spectrophotometer. Since the maximum PL intensity of f-$WS_2$-QDs was observed at 410 nm ($\lambda_{ex}$ ∼ 310 nm) having Stokes shift of 8162 $cm^{-1}$, metal ion sensing application of f-$WS_2$-QDs has been performed at 410 nm. The quantum yield of f-$WS_2$-QDs with respect to anthracene as a reference was estimated by using eq 1 in Supporting Information and was found to be $\Phi_{WS_2}$ ∼ 4.04%, which is comparable to the $WS_2$-QDs obtained through the liquid phase exfoliation.[9]

The interaction studies have been performed by addition of 180 $\mu$M of different metal ions to the solution of f-$WS_2$-QDs separately. Interaction study showed that fluorescence intensity of f-$WS_2$-QDs centered at 410 nm quenched 60−75% with the addition of $Fe^{2+}$, $Hg^{2+}$, $Cd^{2+}$, $Pb^{2+}$, and $Cu^{2+}$, while it was quenched completely (∼98%) in the presence of $Fe^{3+}$ (Figure 5a). Percentage change in fluorescence intensity ($\Delta F$, %) in the presence of various metal ions is shown in Figure 5b, which also showed that PL intensity is totally quenched in the presence of $Fe^{3+}$ ions. The change in fluorescence intensity of


DOI: 10.1021/acsanm.8b02162
ACS Appl. Nano Mater. 2019, 2, 566−576

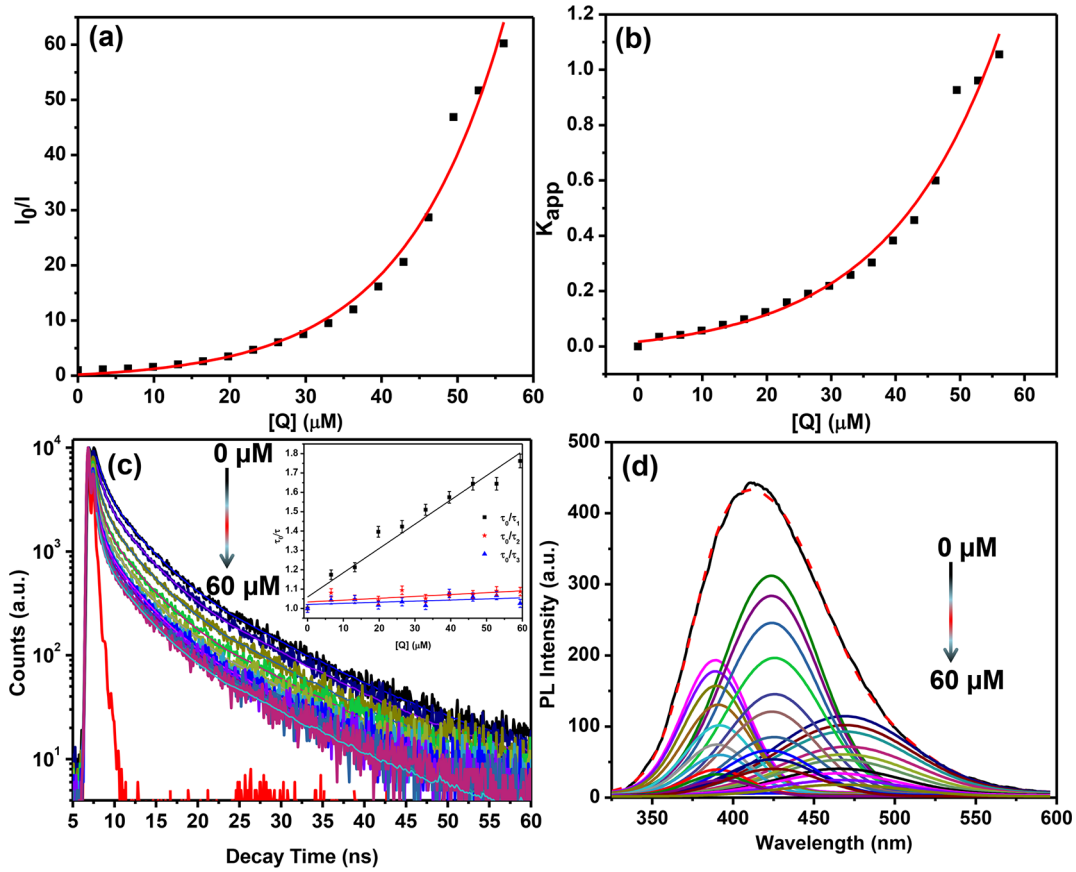


**Figure 6.** (a, b) Stern−Volmer plot, showing exponential increment in PL intensity ratio with the gradual addition of $Fe^{3+}$ ions into the f-$WS_2$-QDs solution. (c) Picosecond time-resolved fluoroscence transient of fluorophore (f-$WS_2$-QDs), showing decrement in lifetime with the addition of quencher ($Fe^{3+}$) from 0 to 60 $\mu$M, under laser excitation of 375 nm, and inset showing the relative change in average lifetimes with the successive addition of $Fe^{3+}$ ions. (d) Deconvoluted PL spectra corresponding to increasing $Fe^{3+}$ concentration showing the presence of three types of quenching species.

f-$WS_2$-QDs in the presence of $Fe^{2+}$, $Hg^{2+}$, $Cd^{2+}$, $Pb^{2+}$, and $Cu^{2+}$ may be attributed to the adsorption of these metal ions on the surface of f-$WS_2$-QDs.

In order to check the selectivity of sensing probe (f-$WS_2$-QDs) toward $Fe^{3+}$ ions, the competitive metal ion interference experiments were performed with addition of $Fe^{3+}$ in the solution of f-$WS_2$-QDs containing different metal ions and reversibly, upon addition of different metal ions (in excess, ~200.0 $\mu$M) to a solution of f-$WS_2$-QDs-$Fe^{3+}$. The insignificant change in emission intensity of f-$WS_2$-QDs-$Fe^{3+}$ was observed, which suggests the high selectivity of f-$WS_2$-QDs for $Fe^{3+}$ (Figure 5c). Further, to check the sensitivity of sensing probe toward $Fe^{3+}$ ions, emission based titration experiments have also been performed by gradual addition of different concentrations (from 0 $\mu$M to 180 $\mu$M, in step of 3.3 $\mu$M) of $Fe^{3+}$ ion to the solution of f-$WS_2$-QDs. It shows that the emission intensity of f-$WS_2$-QDs centered at 410 nm decreases and reached saturation limit up to addition of 180 $\mu$M $Fe^{3+}$ ion (Figure 5d) and quantum yield decreases from ~4.04% to ~0.1% (Table S1).

Further, the detection limit of f-$WS_2$-QDs for $Fe^{3+}$ was estimated from the respective fluorescence titration data based on the reported method.[36,37] According to the result of titration experiment, change in the fluorescence intensity of f-$WS_2$-QDs with $Fe^{3+}$ was normalized in between the minimum to maximum intensity. A linear regression curve was obtained from the plot of these normalized fluorescence intensity of f-$WS_2$-QDs with $Fe^{3+}$ versus log [$Fe^{3+}$] (Figure S2), and detection limit was calculated by using eq 1. Limit of detection was found to be as low as 1.32 $\mu$M. The plot of PL intensity on log scale versus the quencher ($Fe^{3+}$) concentration (shown in Figure S3) shows that the response of sensor is linear in the range of 0−55 $\mu$M.

$$\mathrm{LOD} = 10^{-[\mathrm{slope/intercept}]} \quad (1)$$

As it is well-known that depending on the nature of fluorescence probe and quencher, quenching of PL intensity may occur due to the formation of complex in ground state (static quenching) or through the diffusion collision process (dynamic quenching). So in order to unveil the fluorescence quenching behavior of f-$WS_2$-QDs in the presence of $Fe^{3+}$, the relative change in fluorescence intensity ($I_0/I$) has been plotted as a function of quencher concentration ([Q]) of $Fe^{3+}$ described by Stern−Volmer (S−V) eq 2 and has been shown in Figure 6a, where $K_{SV}$ is the S−V quenching constant.

$$\frac{I_0}{I} = 1 + K_{SV}[\mathrm{Q}] \quad (2)$$

In the present case, it is observed that relative fluorescence intensity deviates from linearity toward the $y$-axis with the successive addition of $Fe^{3+}$. This indicates that more than one type of quenching processes (static/dynamic quenching) are involved here. So by considering both the quenching processes, we plotted the modified S−V plot governed by eq 3, shown in



DOI: 10.1021/acsanm.8b02162
ACS Appl. Nano Mater. 2019, 2, 566−576

**Table 1. Comparison of the Performance of Various Sensing Probes for the Detection of $Fe^{3+}$**

| SN | sensing probe | linearity | detection limit | $K_{SV}$ ($M^{-1}$) | ref |
|---|---|---|---|---|---|
| 1. | CQDs | 12.5−100 $\mu$M | 9.79 $\mu$M | $3.148 \times 10^3$ | 39 |
| 2 | iridium(III)-based metal−organic frameworks | | 1.215 $\mu$M | $1.165 \times 10^4$ | 40 |
| 3 | dopamine functionalized GQDs | 20 nM to 2 $\mu$M | 7.6 $\mu$M | | 41 |
| 4 | N, P co-doped CQDs | 20−200 $\mu$M | 20.0 $\mu$M | | 42 |
| 5 | gold nanoclusters (AuNCs) | 5.0−1280 $\mu$M | 3.5 $\mu$M | | 43 |
| 6 | nitrogen-doped carbon dots | 0.5−1000 $\mu$M | 79 nM | | 44 |
| 7 | N, S CQDs | 25−500 $\mu$M | 4.0 $\mu$M | $2.85 \times 10^3$ | 45 |
| 8 | f-$WS_2$-QDs | 0−55 $\mu$M | 1.32 $\mu$M | $1.1 \times 10^4$ | present work |

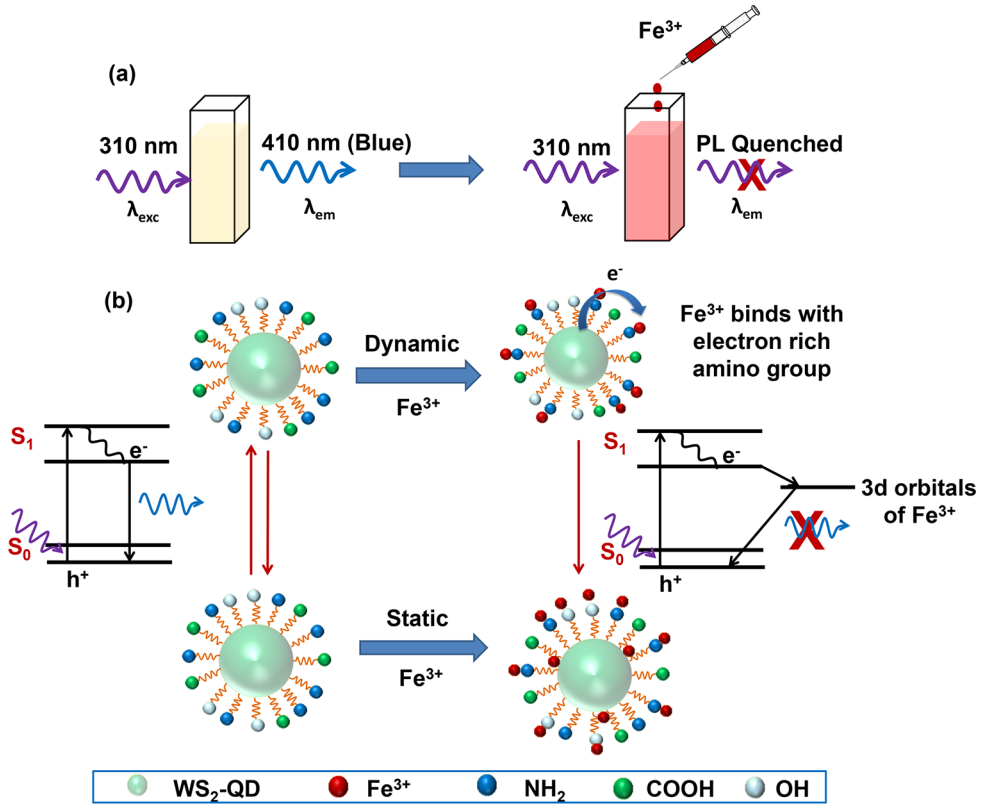


**Figure 7.** (a) and (b) showing the schematic representations of the fluorescence quenching of f-$WS_2$-QDs in the presence of $Fe^{3+}$ ions and process of dynamic quenching and static quenching, respectively.

Figure 6b, where $K_D$ and $K_S$ are dynamic and static quenching constants.

$$K_{app} = \frac{\left(\frac{I_0}{I} - 1\right)}{[Q]} = (K_D + K_S) + K_D K_S[Q] \quad (3)$$

In this case again a positive deviation from S−V equation has been observed. This indicates that along with a ground state complex, few fluorophores are also present that do not form ground state complex but instead are quenched due to the presence of quencher in the close vicinity of fluorophore at the time of excitation. These closely spaced fluorophore−quencher pairs are quenched immediately at the time of excitation, resulting in dark complexes.[38] The formation of dark complexes in ground state is also supported from the absorption data of f-$WS_2$-QDs solution with gradual addition of $Fe^{3+}$ ions, shown in Figure S4. From here it can be predicted that three types of fluorophores exist in the solution in which one is quenched through collisional and other two shows quenching in ground state.

Further, the specified quenching behavior can be determined through the time-resolved photoluminescence (TRPL) measurement. In order to distinguish the quenching behavior (dynamic/static), TRPL measurement was also carried out. Figure 6c represents the picosecond time-resolved transient with the successive addition of $Fe^{3+}$ ion from 0 to 60 $\mu$M. It is observed from the fluorescence transients of f-$WS_2$-$QD_S$-$Fe^{3+}$ system that the average lifetime ($\tau$) decreases with the addition of $Fe^{3+}$. The exciton lifetime in TRPL measurement is fitted with eq 2 in Supporting Information, and it shows the triexponential decays. Lifetime corresponding to each triexponential decay ($\tau_1$, $\tau_2$, and $\tau_3$) has been summarized in Table S2, and this triexponential decay signifies the presence of three types of fluorescing sites (as observed from modified S−V plot) present in the f-$WS_2$-QDs solution. It is observed that lifetime ($\tau_1$) decreases from 0.74 to 0.42 ns with the increasing concentration of quencher ($Fe^{3+}$) from 0 $\mu$M to 60 $\mu$M. However, the decay times $\tau_2$, and $\tau_3$ remain nearly constant. Further, variation in relative change of fluorescence lifetime has been represented in the inset of Figure 6c. From here it is


DOI: 10.1021/acsanm.8b02162
ACS Appl. Nano Mater. 2019, 2, 566−576

evident that relative change in fluorescence lifetime corresponding to $\tau_1$ shows linear variation and corresponding to $\tau_2$ and $\tau_3$ remaining nearly constant with increasing concentration of $Fe^{3+}$ and fitted well with the eq 4.

$$\frac{\tau_0}{\tau} = 1 + K_q\tau_0[Q] = 1 + K_D[Q] \quad (4)$$

where $K_q$ is the bimolecular quenching constant. From the slope of S−V plot in Figure 6c using eq 4, the obtained value of $K_D$ is $1.1 \times 10^4$ $M^{-1}$. This indicates that ∼9.1 $\mu$M concentration of $Fe^{3+}$ will be required to quench the 50% intensity of f-$WS_2$-QDs solution. The bimolecular quenching constant $K_q = 1.48 \times 10^{13}$ $M^{-1}$ $s^{-1}$ has been obtained using the values of fluorescence lifetime ($\tau_0$) and S−V constant ($K_D$). The large value of $K_q$ indicates the high efficiency of quenching and accessibility of the fluorophore to the quencher. Further, to verify the presence of three types of quenching species as obtained from TRPL characterization, PL spectra for different concentration of $Fe^{3+}$ are deconvoluted and presented in Figure 6d. From here we can also see that each PL spectrum can be deconvoluted into three PL peaks, which also supports the presence of three types of quenching sites.

Various parameters obtained in the present work have been summarized in Table 1 and compared with other similar works, which suggest that our results are comparable to or better than the other reported works.

**Mechanism for Fluorescence Quenching of f-$WS_2$-QDs in the Presence of $Fe^{3+}$.** As discussed above from PL and TRPL data, we can conclude that the fluorescence quenching is taking place through both dynamic and static quenching process. Both quenching phenomena have been schematically represented in Figure 7. We hypothesized that the apparent static quenching can be attributed to the formation of iron hydroxide in ground state due to the presence of hydroxyl functional group over the surface of f-$WS_2$-QDs and also due to presence of $Fe^{3+}$ in close proximity of f-$WS_2$-QDs.[46] However, the dynamic quenching can be attributed to the coordination of electron deficient $Fe^{3+}$ with the electron (lone pair) rich amino groups present on the surface of f-$WS_2$-QDs in the excited state. Further, this coordination will support the electron transfer from the excited state $S_1$ of the f-$WS_2$-QDs to the half-filled 3d orbitals of $Fe^{3+}$. Now, since electron transfer from 3d orbitals of $Fe^{3+}$ to the $S_0$ orbitals of f-$WS_2$-QDs is forbidden according to the selection rule, this leads to significant fluorescence quenching of f-$WS_2$-QDs.[47]

## CONCLUSIONS

In summary, we demonstrated the "bottom-up" single-step hydrothermal growth of in situ functionalized fluorescent $WS_2$-QDs (average size of ∼5 nm), which are highly stable in aqueous medium without any subsequent treatments. Various structural and spectroscopic characterization techniques including TEM, HR-TEM, AFM, FT-IR, XPS, and Raman demonstrated that f-$WS_2$-QDs are few layered in nature having functional groups over its surface. The as-synthesized f-$WS_2$-QDs exhibited highly intense blue PL emission at $\lambda_{em}$ ∼ 410 nm with an excitation wavelength of $\lambda_{ex}$ ∼ 310 nm with a high PL quantum yield ($\Phi_{WS_2}$ ∼ 4.04%). This fluorescing nature of f-$WS_2$-QDs was successfully applied to devise an optical sensor for highly sensitive and selective detection of $Fe^{3+}$ ions. Its fluorescence was quenched by ∼98% upon interacting with $Fe^{3+}$. Further, we elucidated in detail the fluorescence quenching kinetics of f-$WS_2$-QDs in the presence of $Fe^{3+}$ ions. S−V plot (from PL titration data) and TRPL characterization revealed that the fluorescence quenching of f-$WS_2$-QDs is a mixed phenomenon of both static and dynamic in nature. The sensor response was found to be linear in the range of 0−55 $\mu$M with a lower detection limit of 1.32 $\mu$M, which is comparable to or better than those reported for the other fluorescent sensors for $Fe^{3+}$. Apart from this, S−V quenching constant $K_D = 1.1 \times 10^4$ $M^{-1}$ was also calculated, which indicates that ∼9.1 $\mu$M concentration of $Fe^{3+}$ would be required to quench 50% intensity of f-$WS_2$-QDs solution and larger value of $K_q = 1.48 \times 10^{13}$ $M^{-1}$ $s^{-1}$ indicates the high efficiency of quenching and accessibility of the fluorophore to the quencher. Hence, we believe that present investigation opened up a new avenue for the in situ growth of functionalized QDs with a potential for wide range of applications such as optical sensing, biosensing, and bioimaging, etc.

## ASSOCIATED CONTENT

### Supporting Information

The Supporting Information is available free of charge on the ACS Publications website at DOI: 10.1021/acsanm.8b02162.

FT-IR analysis of f-$WS_2$-QDs, quantum yield calculation of f-$WS_2$-QDs, LOD and linearity plot for the proposed optical sensor, UV−vis absorption titration data, and table containing decay life times of f-$WS_2$-QDs with increasing concentrations of $Fe^{3+}$ ions (PDF)

## AUTHOR INFORMATION


### Corresponding Authors

*R.S.T.: e-mail, rstiwariphy@yahoo.com; phone, +91-9415991746.

*A.S.: e-mail, anchalbhu@gmail.com; phone, +91-9453203122.

### ORCID

Arvind Misra: 0000-0003-2716-4139

Anchal Srivastava: 0000-0002-5804-6840


### Notes

The authors declare no competing financial interest.

## ACKNOWLEDGMENTS

V.K.S. acknowledges the UGC for providing Senior Research Fellowship (Fellowship Grant F.25-1/2014-15/(BSR)/5-127/2007/(BSR)). H.M. is thankful to CSIR, New Delhi, for providing an SRF fellowship (Fellowship Grant 09/013(0752)/2018-EMR-I). A.S. acknowledges DST, India (Project DST/TSG/PT/2012/68), DST-PURSE, SERB, India (Project EMR/2016/007720), and CAS-BHU for providing financial support. The authors acknowledge Bio-Physics Laboratory of Physics Department, Institute of Science, BHU, for access to the facilities for UV−vis, PL, and TRPL measurements.

## REFERENCES

(1) Coleman, J. N.; Lotya, M.; O'Neill, A.; Bergin, S. D.; King, P. J.; Khan, U.; Young, K.; Gaucher, A.; De, S.; Smith, R. J.; et al. Two-Dimensional Nanosheets Produced by Liquid Exfoliation of Layered Materials. *Science* **2011**, *331*, 568−571.

(2) Chhowalla, M.; Shin, H. S.; Eda, G.; Li, L.-J.; Loh, K. P.; Zhang, H. The Chemistry of Two-Dimensional Layered Transition Metal Dichalcogenide Nanosheets. *Nat. Chem.* **2013**, *5*, 263.
(3) Xu, M.; Liang, T.; Shi, M.; Chen, H. Graphene-Like Two-Dimensional Materials. *Chem. Rev.* **2013**, *113*, 3766−3798.
(4) Butler, S. Z.; Hollen, S. M.; Cao, L.; Cui, Y.; Gupta, J. A.; Gutiérrez, H. R.; Heinz, T. F.; Hong, S. S.; Huang, J.; Ismach, A. F.; et al. Progress, Challenges, and Opportunities in Two-Dimensional Materials Beyond Graphene. *ACS Nano* **2013**, *7*, 2898−2926.
(5) Gutiérrez, H. R.; Perea-López, N.; Elías, A. L.; Berkdemir, A.; Wang, B.; Lv, R.; López-Urías, F.; Crespi, V. H.; Terrones, H.; Terrones, M. Extraordinary Room-Temperature Photoluminescence in Triangular $WS_2$ Monolayers. *Nano Lett.* **2013**, *13*, 3447−3454.
(6) Zhao, W.; Ghorannevis, Z.; Chu, L.; Toh, M.; Kloc, C.; Tan, P.-H.; Eda, G. Evolution of Electronic Structure in Atomically Thin Sheets of $WS_2$ and $WSe_2$. *ACS Nano* **2013**, *7*, 791−797.
(7) Jariwala, D.; Sangwan, V. K.; Lauhon, L. J.; Marks, T. J.; Hersam, M. C. Emerging Device Applications for Semiconducting Two-Dimensional Transition Metal Dichalcogenides. *ACS Nano* **2014**, *8*, 1102−1120.
(8) Molina-Sanchez, A.; Wirtz, L. Phonons in Single-Layer and Few-Layer $MoS_2$ and $WS_2$. *Phys. Rev. B: Condens. Matter Mater. Phys.* **2011**, *84*, 155413.
(9) Lin, L.; Xu, Y.; Zhang, S.; Ross, I. M.; Ong, A. C.; Allwood, D. A. Fabrication of Luminescent Monolayered Tungsten Dichalcogenides Quantum Dots with Giant Spin-Valley Coupling. *ACS Nano* **2013**, *7*, 8214−8223.
(10) Yan, Y.; Zhang, C.; Gu, W.; Ding, C.; Li, X.; Xian, Y. Facile Synthesis of Water-Soluble $WS_2$ Quantum Dots for Turn-On Fluorescent Measurement of Lipoic Acid. *J. Phys. Chem. C* **2016**, *120*, 12170−12177.
(11) Xu, S.; Li, D.; Wu, P. One-Pot, Facile, and Versatile Synthesis of Monolayer $MoS_2/WS_2$ Quantum Dots as Bioimaging Probes and Efficient Electrocatalysts for Hydrogen Evolution Reaction. *Adv. Funct. Mater.* **2015**, *25*, 1127−1136.
(12) Zhang, X.; Lai, Z.; Liu, Z.; Tan, C.; Huang, Y.; Li, B.; Zhao, M.; Xie, L.; Huang, W.; Zhang, H. A Facile and Universal Top-Down Method for Preparation of Monodisperse Transition-Metal Dichalcogenide Nanodots. *Angew. Chem., Int. Ed.* **2015**, *54*, 5425−5428.
(13) Nicolosi, V.; Chhowalla, M.; Kanatzidis, M. G.; Strano, M. S.; Coleman, J. N. Liquid Exfoliation of Layered Materials. *Science* **2013**, *340*, 1226419.
(14) Yong, Y.; Cheng, X.; Bao, T.; Zu, M.; Yan, L.; Yin, W.; Ge, C.; Wang, D.; Gu, Z.; Zhao, Y. Tungsten Sulfide Quantum Dots as Multifunctional Nanotheranostics for In Vivo Dual-Modal Image-Guided Photothermal/Radiotherapy Synergistic Therapy. *ACS Nano* **2015**, *9*, 12451−12463.
(15) Bai, X.; Wang, J.; Mu, X.; Yang, J.; Liu, H.; Xu, F.; Jing, Y.; Liu, L.; Xue, X.; Dai, H.; Liu, Q.; Sun, Y.-M.; Liu, C.; Zhang, X.-D. Ultrasmall $WS_2$ Quantum Dots with Visible Fluorescence for Protection of Cells and Animal Models from Radiation-Induced Damages. *ACS Biomater. Sci. Eng.* **2017**, *3*, 460−470.
(16) Gan, Z.; Liu, L.; Wu, H.; Hao, Y.; Shan, Y.; Wu, X.; Chu, P. K. Quantum Confinement Effects Across Two-Dimensional Planes in $MoS_2$ Quantum Dots. *Appl. Phys. Lett.* **2015**, *106*, 233113.
(17) Noh, M.; Kim, T.; Lee, H.; Kim, C.-K.; Joo, S.-W.; Lee, K. Fluorescence Quenching Caused by Aggregation of Water-Soluble CdSe Quantum Dots. *Colloids Surf., A* **2010**, *359*, 39−44.
(18) Sahoo, S. K.; Sharma, D.; Bera, R. K.; Crisponi, G.; Callan, J. F. Iron (III) Selective Molecular and Supramolecular Fluorescent Probes. *Chem. Soc. Rev.* **2012**, *41*, 7195−7227.
(19) Papanikolaou, G.; Samuels, M. E.; Ludwig, E. H.; MacDonald, M. L.; Franchini, P. L.; Dubé, M.-P.; Andres, L.; MacFarlane, J.; Sakellaropoulos, N.; Politou, M.; et al. Mutations in HFE2 Cause Iron Overload in Chromosome 1q-Linked Juvenile Hemochromatosis. *Nat. Genet.* **2004**, *36*, 77.
(20) Ong, W.-Y.; Farooqui, A. A. Iron, Neuroinflammation, and Alzheimer's Disease. *J. Alzheimer's Dis.* **2005**, *8*, 183−200.
(21) Tesfaldet, Z. O.; van Staden, J. F.; Stefan, R. I. Sequential Injection Spectrophotometric Determination of Iron as Fe(II) in Multi-Vitamin Preparations Using 1,10-Phenanthroline as Complexing Agent. *Talanta* **2004**, *64*, 1189−1195.
(22) Bobrowski, A.; Nowak, K.; Zarębski, J. Application of a Bismuth Film Electrode to the Voltammetric Determination of Trace Iron Using a Fe (III)−TEA−$BrO_3$− Catalytic System. *Anal. Bioanal. Chem.* **2005**, *382*, 1691−1697.
(23) Yokoi, K.; van den Berg, C. M. The Determination of Iron in Seawater Using Catalytic Cathodic Stripping Voltammetry. *Electroanalysis* **1992**, *4*, 65−69.
(24) Valeur, B.; Leray, I. Design Principles of Fluorescent Molecular Sensors for Cation Recognition. *Coord. Chem. Rev.* **2000**, *205*, 3−40.
(25) Wang, Y.; Ni, Y. Molybdenum Disulfide Quantum Dots as a Photoluminescence Sensing Platform for 2, 4, 6-Trinitrophenol Detection. *Anal. Chem.* **2014**, *86*, 7463−7470.
(26) Mishra, H.; Umrao, S.; Singh, J.; Srivastava, R. K.; Ali, R.; Misra, A.; Srivastava, A. pH Dependent Optical Switching and Fluorescence Modulation of Molybdenum Sulfide Quantum Dots. *Adv. Opt. Mater.* **2017**, *5*, 1601021.
(27) Li, X.; He, D.-W.; Wang, Y.-S.; Hu, Y.; Zhao, X.; Fu, C.; Wu, J.-Y. Facile and Controllable Synthesis of Molybdenum Disulfide Quantum Dots for Highly Sensitive and Selective Sensing of Copper Ions. *Chin. Phys. B* **2018**, *27*, No. 056104.
(28) Atkin, P.; Daeneke, T.; Wang, Y.; Carey, B.; Berean, K.; Clark, R.; Ou, J.; Trinchi, A.; Cole, I.; Kalantar-Zadeh, K. 2D $WS_2$/Carbon Dot Hybrids with Enhanced Photocatalytic Activity. *J. Mater. Chem. A* **2016**, *4*, 13563−13571.
(29) Ghorai, A.; Bayan, S.; Gogurla, N.; Midya, A.; Ray, S. K. Highly Luminescent $WS_2$ Quantum Dots/ZnO Heterojunctions for Light Emitting Devices. *ACS Appl. Mater. Interfaces* **2017**, *9*, 558−565.
(30) Zeng, H.; Liu, G.-B.; Dai, J.; Yan, Y.; Zhu, B.; He, R.; Xie, L.; Xu, S.; Chen, X.; Yao, W.; Cui, X. Optical Signature of Symmetry Variations and Spin-Valley Coupling in Atomically Thin Tungsten Dichalcogenides. *Sci. Rep.* **2013**, *3*, 1608.
(31) Martinez, H.; Benayad, A.; Gonbeau, D.; Vinatier, P.; Pecquenard, B.; Levasseur, A. Influence of The Cation Nature of High Sulfur Content Oxysulfide Thin Films Moysz (M= W, Ti) Studied by XPS. *Appl. Surf. Sci.* **2004**, *236*, 377−386.
(32) Audi, A. A.; Sherwood, P. X-Ray Photoelectron Spectroscopic Studies of Sulfates and Bisulfates Interpreted by $X_\alpha$ and Band Structure Calculations. *Surf. Interface Anal.* **2000**, *29*, 265−275.
(33) Volynsky, A. B.; Stakheev, A. Y.; Telegina, N. S.; Senin, V. G.; Kustov, L. M.; Wennrich, R. Low-Temperature Transformations of Sodium Sulfate and Sodium Selenite in the Presence of Pre-Reduced Palladium Modifier in Graphite Furnaces for Electrothermal Atomic Absorption Spectrometry. *Spectrochim. Acta, Part B* **2001**, *56*, 1387−1396.
(34) Hsieh, C.-T.; Tzou, D.-Y.; Hsieh, K.-Y.; Yin, K.-M. Photoluminescence from Amino Functionalized Graphene Quantum Dots Prepared by Electrochemical Exfoliation Method in the Presence of Ammonium Ions. *RSC Adv.* **2017**, *7*, 18340−18346.
(35) Bertus, L.; Faure, C.; Danine, A.; Labrugère, C.; Campet, G.; Rougier, A.; Duta, A. Synthesis and Characterization of $WO_3$ Thin Films by Surfactant Assisted Spray Pyrolysis for Electrochromic Applications. *Mater. Chem. Phys.* **2013**, *140*, 49−59.
(36) Shortreed, M.; Kopelman, R.; Kuhn, M.; Hoyland, B. Fluorescent Fiber-Optic Calcium Sensor for Physiological Measurements. *Anal. Chem.* **1996**, *68*, 1414−1418.
(37) Kim, M. H.; Jang, H. H.; Yi, S.; Chang, S.-K.; Han, M. S. Coumarin-Derivative-Based Off−On Catalytic Chemodosimeter for $Cu^{2+}$ Ions. *Chem. Commun.* **2009**, 4838−4840.
(38) Mahata, P.; Mondal, S. K.; Singha, D. K.; Majee, P. Luminescent Rare-Earth-Based Mofs as Optical Sensors. *Dalton Transactions* **2017**, *46*, 301−328.
(39) Aslandaş, A. M.; Balcı, N.; Arık, M.; Şakiroğlu, H.; Onganer, Y.; Meral, K. Liquid Nitrogen-Assisted Synthesis of Fluorescent Carbon Dots from Blueberry and their Performance in $Fe^{3+}$ Detection. *Appl. Surf. Sci.* **2015**, *356*, 747−752.


DOI: 10.1021/acsanm.8b02162
*ACS Appl. Nano Mater.* 2019, 2, 566−576

(40) Fan, K.; Bao, S.-S.; Nie, W.-X.; Liao, C.-H.; Zheng, L.-M. Iridium(III)-Based Metal−Organic Frameworks as Multiresponsive Luminescent Sensors for $Fe^{3+}$, $Cr_2O_7^{2-}$, and $ATP^{2-}$ in Aqueous Media. *Inorg. Chem.* **2018**, *57*, 1079−1089.
(41) Dutta Chowdhury, A.; Doong, R.-a. Highly Sensitive and Selective Detection of Nanomolar Ferric Ions Using Dopamine Functionalized Graphene Quantum Dots. *ACS Appl. Mater. Interfaces* **2016**, *8*, 21002−21010.
(42) Chandra, S.; Laha, D.; Pramanik, A.; Ray Chowdhuri, A.; Karmakar, P.; Sahu, S. K. Synthesis of Highly Fluorescent Nitrogen and Phosphorus Doped Carbon Dots for the Detection of $Fe^{3+}$ Ions In Cancer Cells. *Luminescence* **2016**, *31*, 81−87.
(43) Annie Ho, J.-a.; Chang, H.-C.; Su, W.-T. DOPA-Mediated Reduction Allows the Facile Synthesis of Fluorescent Gold Nanoclusters for Use as Sensing Probes for Ferric Ions. *Anal. Chem.* **2012**, *84*, 3246−3253.
(44) Lv, P.; Yao, Y.; Zhou, H.; Zhang, J.; Pang, Z.; Ao, K.; Cai, Y.; Wei, Q. Synthesis of Novel Nitrogen-Doped Carbon Dots for Highly Selective Detection of Iron Ion. *Nanotechnology* **2017**, *28*, 165502.
(45) Ding, H.; Wei, J.-S.; Xiong, H.-M. Nitrogen and Sulfur Co-Doped Carbon Dots with Strong Blue Luminescence. *Nanoscale* **2014**, *6*, 13817−13823.
(46) Zhu, X.; Zhang, Z.; Xue, Z.; Huang, C.; Shan, Y.; Liu, C.; Qin, X.; Yang, W.; Chen, X.; Wang, T. Understanding the Selective Detection of $Fe^{3+}$ Based on Graphene Quantum Dots as Fluorescent Probes: the $K_{sp}$ of a Metal Hydroxide-Assisted Mechanism. *Anal. Chem.* **2017**, *89*, 12054−12058.
(47) Wu, Q.; Wang, X.; Jiang, Y.; Sun, W.; Wang, C.; Yang, M.; Zhang, C. $MoS_2$-QD-Based Dual-Model Photoluminescence Sensing Platform for Effective Determination of $Al^{3+}$ and $Fe^{3+}$ Simultaneously in Various Environment. *ChemistrySelect* **2018**, *3*, 2326−2331.



DOI: 10.1021/acsanm.8b02162
*ACS Appl. Nano Mater.* 2019, 2, 566−576